Taylor & Francis
Taylor & Francis Group

RESEARCH PAPER

OPEN ACCESS | Check for updates

Moonlighting of *Haemophilus influenzae* heme acquisition systems contributes to the host airway-pathogen interplay in a coordinated manner

Irene Rodríguez-Arce[a]*, Tamim Al-Jubair [b,c]*, Begoña Euba[a,d], Ariadna Fernández-Calvet [a], Celia Gil-Campillo[a], Sara Martí[d,e], Susanna Törnroth-Horsefield[f], Kristian Riesbeck [b], and Junkal Garmendia[a,d]

aInstituto de Agrobiotecnología, CSIC-Gobierno, Navarra, Spain; bClinical Microbiology, Department of Translational Medicine, Faculty of Medicine, Lund University, Malmö, Sweden; cDepartment of Biomedical Sciences, Faculty of Health Sciences, University of Copenhagen, Copenhagen, Denmark; dCentro de Investigación Biomédica en Red de Enfermedades Respiratorias (CIBERES), Madrid, Spain; eDepartamento Microbiología, Hospital Universitari Bellvitge, University of Barcelona, IDIBELL, Barcelona, Spain; fDepartment of Biochemistry and Structural Biology, Center for Molecular Protein Science, Lund University, Lund, Sweden

ABSTRACT

Nutrient iron sequestration is the most significant form of nutritional immunity and causes bacterial pathogens to evolve strategies of host iron scavenging. Cigarette smoking contains iron particulates altering lung and systemic iron homeostasis, which may enhance colonization in the lungs of patients suffering chronic obstructive pulmonary disease (COPD) by opportunistic pathogens such as nontypeable. NTHi is a heme auxotroph, and the NTHi genome contains multiple heme acquisition systems whose role in pulmonary infection requires a global understanding. In this study, we determined the relative contribution to NTHi airway infection of the four heme-acquisition systems HxuCBA, PE, SapABCDFZ, and HbpA-DppBCDF that are located at the bacterial outer membrane or the periplasm. Our computational studies provided plausible 3D models for HbpA, SapA, PE, and HxuA interactions with heme. Generation and characterization of single mutants in the *hxuCBA, hpe, sapA,* and *hbpA* genes provided evidence for participation in heme binding-storage and inter-bacterial donation. The *hxuA, sapA, hbpA,* and *hpe* genes showed differential expression and responded to heme. Moreover, HxuCBA, PE, SapABCDFZ, and HbpA-DppBCDF presented moonlighting properties related to resistance to antimicrobial peptides or glutathione import, together likely contributing to the NTHi-host airway interplay, as observed upon cultured airway epithelia and *in vivo* lung infection. The observed multi-functionality was shown to be system-specific, thus limiting redundancy. Together, we provide evidence for heme uptake systems as bacterial factors that act in a coordinated and multi-functional manner to subvert nutritional- and other sources of host innate immunity during NTHi airway infection.

Introduction

The need of invading bacteria to acquire nutrient metals from their environments has caused vertebrate hosts to evolve to restrict their bioavailability. Nutrient iron sequestration is one mode of innate defence termed "iron nutritional immunity", whereby iron levels are tightly controlled by host regulatory systems controlling its absorption, systemic transport, distribution, cellular uptake, and storage [1,2]. In response to this, pathogens evolve mechanisms of host iron piracy to scavenge this metal during infection [3].

Iron exists in the reduced ferrous (Fe^{2+}) or oxidized ferric (Fe^{3+}) forms. The Fe^{2+}/Fe^{3+} redox potential makes it extremely versatile when incorporated into proteins as a catalytic center or electron carrier, and it is essential in numerous biological processes. Although abundant in nature, iron does not normally occur in its biologically active ferrous form. Under aerobic conditions, Fe^{2+} is unstable and generates Fe^{3+} and reactive oxygen species (ROS) via the Fenton reaction, the latter of which can damage lipids, DNA, and proteins [4]. Conversely, ferric iron is poorly water-soluble and requires specialized proteins to facilitate its mobilization and maintain intracellular reservoir (lactoferrin and transferrin for transport, ferritin for storage). However, the most abundant form of iron in vertebrates is bound within a porphyrin ring as ferriprotoporphyrin IX (heme) [5], most of which is bound to intracellular proteins (hemoglobin, myoglobin, cytochromes). Hemoglobin from lysed erythrocytes is bound by haptoglobin, whereas free heme is bound to hemopexin and, to a lesser extent, to albumin, under which circumstances it may become available to

---

*These authors contributed equally to this work
⊞ Supplemental data for this article can be accessed here.

extracellular pathogens [6]. Many pathogens thus exploit host heme as a nutrient iron source [5,7,8].

In the lungs, iron is stored in ferritin, macrophages sequester heme from senescent erythrocytes, take and store iron from transferrin, and clear inhaled iron-containing particulate matter. Likewise, neutrophils release iron regulatory molecules helping sequester free iron [9–11]. Human lung iron levels range between 0.4–0.9 mg/g, and ~10 μg iron are exposed to lungs daily at a normal rate of breathing from the atmosphere [12]. Exposure to higher iron levels through inhalation of iron-containing particulate matter provides catalytically active iron resulting in tissue damage. Moreover, alveolar hemorrhaging observed in several lung disease conditions leads to increased iron levels. As a consequence, strong evidence for dysregulated iron homeostasis exists in major respiratory diseases including chronic obstructive pulmonary disease (COPD) [1,2,13–15]. COPD is a complex progressive condition characterized by chronic airway inflammation, associated with airway remodeling, alveolar destruction and persistent airflow obstruction [16]. Cigarette smoking, the single greatest risk factor for developing COPD [17], contains iron particulates inducing intracellular iron accumulation [13,14]. Elevated levels of iron, ferritin, and oxidative stress are found in the lungs of smokers, where alveolar macrophages increase iron loading [13,14,18–20]. Similarly, the COPD airways present altered levels of iron-binding proteins, increased iron loading by alveolar macrophages, and high rates of polymorphisms in genes associated with iron regulation [21–28]. Given that iron overload increases the virulence of numerous pathogens [29,30], dysregulation of iron homeostasis in the COPD lungs may also facilitate persistence by opportunistic pathogens in the lower airways [2,6,11].

Nontypeable *Haemophilus influenzae* (NTHi) is typically a commensal of the human upper airways, but also a common opportunistic pathogen in the lower airways of patients with COPD [31–35]. NTHi persistence within the COPD lungs contributes to airway inflammation that results in worsening of symptoms and promotes disease progression [33,36–38]. NTHi is incapable of synthesizing heme, but possesses a ferrochelatase that reversibly inserts iron into protoporphyrin IX (PPIX) to form heme [39,40]. Thus, it requires either iron in the presence of PPIX or exogenous heme to grow aerobically [41]. NTHi presents a variety of heme uptake-binding systems including TonB-dependent outer membrane systems that bind heme or hemoproteins (Hup [42], HemR [43], Hgps [44–50], HxuCBA [51–56]), and TonB-independent periplasmic proteins that bind heme and are linked to inner membrane ABC transporters (SapABCDFZ, HbpA-DppBCDF [57–62]). NTHi also stores and shares heme by using the outer membrane protein E (PE) [63] (Figure 1). Information on the contribution of heme uptake to NTHi respiratory infection is scattered [47,50,55,60,64], and a global understanding is lacking.

Existing evidence prompted us to hypothesize that pathological disruption of lung iron homeostasis and bacterial heme auxotrophy may have evolved NTHi toward the coordinated action of its repertoire of heme scavenging mechanisms, to evade nutritional immunity and facilitate the host-pathogen interplay. In this study, HxuCBA, PE, SapABCDFZ, and HbpA-DppBCDF were selected as representative *H. influenzae* heme binding systems at the outer membrane and within the periplasm (Figure 1). Systematic bacterial gene inactivation and phenotypic assessment revealed their relative contribution to NTHi airway infection, and their ability to bind heme was investigated *in silico*.

Materials and methods

Computational modeling

Docking of heme B to HbpA, SapA, PE, and HxuA was performed using the HADDOCK2.2 (High
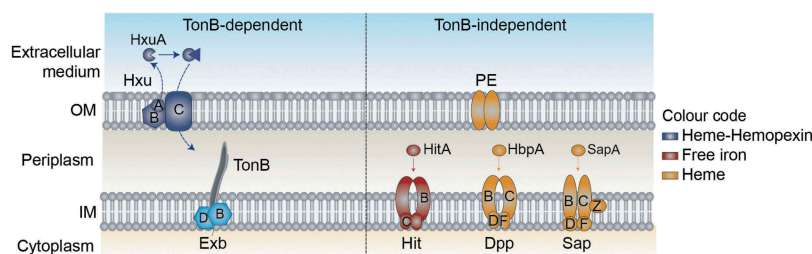
Figure 1. **Schematic representation of NTHi heme uptake systems considered in this study**. HxuCBA is a TonB-dependent system involved in heme-hemopexin binding. HxuC is a receptor and HxuAB is a two-partner secretion system. HxuA is exposed at the cell surface, and leads to heme release and its capture by HxuC. SapABCDFZ, HbpA-DppBCDF and PE are TonB-independent systems. SapA and HbpA are periplasmic proteins that bind heme and are linked to the inner membrane ABC transporters SapBCDFZ and DppBCDF, respectively. PE is an outer membrane protein that binds heme as a dimer. The HitABC free iron uptake system is also shown. HitA is a periplasmic protein that binds free iron linked to the HitBC transporter located at the inner membrane. Heme-iron sources are color-coded.

Ambiguity-Driven protein-protein DOCKing) server [65,66]. For HbpA and SapA, the I-TASSER server [67,68] was used to generate homology models based on the crystal structure of HbpA from *Haemophilus parasuis* in its ligand-bound form (PDB code 3M8U) [62]. For both proteins, the best scoring I-TASSER model was used for the docking experiment. To drive the docking, residues with 60% ligand binding probability as estimated by the COACH function within the I-TASSER suite [69,70] were included as part of an initial estimation of the location of the binding site (residues 61–64, 155, 280, 396, 398, 445–447, and 537 for HbpA; residues 54–55, 458–460, and 462 for SapA). In addition to full-length SapA, heme docking was also performed after removing residues 140–158. For PE, heme was docked to the crystal structure of the PE-dimer (3ZH5). Residues from both monomers within the predicted heme binding pocket (59, 65, 67, 94, 96, 98, 101, 103, and 107) were used to drive the docking. For HxuA, heme was docked to the HxuA crystal structure (PDB code 4RM6), and residues in a manually identified putative binding pocket (450, 452, 464, 516, 526, 556, 560, and 572) were used to drive the docking. Docking solutions were evaluated based on the HADDOCK score and Z-score (the number of standard deviations the HADDOCK score of a given solution is separated from the mean of all clusters). For HbpA, truncated SapA, and PE, a single statistically significant solution cluster was obtained ($p < 0.05$) whereas for HxuA, two equally good solutions were obtained. For full-length SapA, a second solution (cluster 4) with a non-significantly different HADDOCK score from the top solution was obtained. However, this was discarded due to the significantly higher Z-score (−0.2 compared to −1.7 for the top solution). Detailed docking statistics are given in Table S4. The top solution in each cluster was further analyzed in PyMOL (PyMOL Molecular Graphics System, version 2.0, Schrödinger, LLC), and LigPlot$^+$ [71], which were also used to generate figures.

Bacterial strains, plasmids, and growth media

Strains and plasmids used in this study are described in Table 1 and Table S1. NTHi strains were grown for 16 h, at 37°C, 5% CO_2, on chocolate agar (Biomérieux), Mueller Hinton-Fastidious agar (MH-F) (Biomérieux), *Haemophilus* Test Medium agar (HTM, Oxoid), or Brain-Heart Infusion agar (BHI, Oxoid). BHI was supplemented with 10 µg/ml nicotinamide adenine dinucleotide (NAD, factor V) (Sigma-Aldrich) (referred to as BHI-NAD or heme-deficient medium). Alternatively, HTM and BHI were supplemented with both NAD and 10 µg/ml heme (factor X) (Sigma-Aldrich) (referred to as sHTM and sBHI). Liquid cultures were grown in heme-deficient medium, sBHI or, alternatively, in a chemically defined minimal medium (CDMM) supplemented with 50 µM cystine (Sigma-Aldrich) or 50 µM glutathione disulfide (GSSG) (Sigma-Aldrich) (Table S2 [62,72,73]). GSSG (20 mM) was prepared in sterile water; 20 mM cystine was prepared in 1M HCl, filtered and maintained at 4°C until use. Erythromycin (Erm) at 11 µg/ml or spectinomycin (Spec) at 50 µg/ml was used when required. *Escherichia coli* was grown on Luria Bertani (LB) agar at 37°C, supplemented with ampicillin at 100 µg/ml, Erm at 150 µg/ml, or Spec at 50 µg/ml, when indicated.

Table 1. Bacterial strains used in this study.

Strain	Description	Source
H. influenzae		
NTHi375	Wild-type, otitis media clinical isolate	[117]
NTHi375ΔhxuCBA-P682	hxuCBA::spec, Spec^R	This study
NTHi375ΔsapA-1665	sapA::ermC::ermC, Erm^R	This study
NTHi375ΔhbpA-P896	hbpA::spec, Spec^R	This study
NTHi375Δhpe-P897	hpe::spec, Spec^R	This study
RdKW20	Laboratory strain, capsule-deficient serotype d	[97]
RdKW20ΔhxuCBA-P683	hxuCBA::spec, Spec^R	This study
RdKW20ΔsapA-P578	sapA::ermC::ermC, Erm^R	This study
RdKW20ΔhbpA-P885	hbpA::spec, Spec^R	This study
RdKW20ΔhitBC-P804	hitBC::ermC, Erm^R	This study
NTHi3655luxABCDE-P845	Luminiscent strain derived from isolate NTHi3655. It contains a copy of the luxABCDE operon inserted in the genome.	[63]
E. coli		
TOP10	Used for cloning assays	Thermofisher Scientific
SW102	Derived from DY380, it contains a defective λ prophage with the recombination proteins exo, bet, and gam being controlled by the temperature-sensitive repressor cl857	[75]

Generation of H. influenzae *mutant strains*

Plasmids, primers, and construct design are shown in Tables S1, S3, and Fig. S1A. Briefly, a DNA fragment containing each gene/operon and its respective flanking regions was PCR amplified with *Phusion* polymerase (ThermoScientific) using NTHi375 genomic DNA as template and primers gene+flanking region-F1 and gene+flanking region-R1, and cloned into pJET1.2/blunt (ThermoScientific) or pGEMT-easy (Promega), generating plasmids pJET1.2-hxuCBA, pGEMT-sapAB, pJET1.2-hbpA, and pJET1.2-hpe. To generate pJET1.2-hitABC, two DNA fragments of the *hitABC* operon were independently amplified using primers hitABC-F1/hitABC-R2 and hitABC-F2/hitABC-R1, respectively, *Kpn*I digested and ligated, rendering a product with a 853 bp deletion of the *hitB* gene 3′ end and a 200 bp deletion of the *hitC* gene 5′ end, which was further amplified with primers hitABC-F1 and hitABC-R1 and cloned into pJET1.2 to generate pJET1.2-hitABC. An Erm-based disruption strategy was used to generate ΔsapA and ΔhitBC strains. pGEMT-sapAB was disrupted by inverse PCR with *Phusion* polymerase, using primers sapAB-F2 and sapAB-R2. A *sapA* gene internal fragment of 168 bp was replaced by a blunt-ended ErmC resistance cassette excised by *Sma*I digestion from pBSLerm [74], generating pGEMT-sapA::ermC, which was used as a template to amplify the *sapA::ermC* disruption cassette with primers sapAB-F1 and sapAB-R1. pJET1.2-hitABC was *Kpn*I digested and used as cloning vector for a *Kpn*I blunt-ended ErmC resistance gene excised by *Kpn*I digestion from pBSLerm, generating pJET1.2-hitBC::ermC, which was used as a template to amplify the *hitBC::ermC* disruption cassette with primers hitABC-F1 and hitABC-R1. Alternatively, a Spec-based disruption strategy was used to generate ΔhxuCBA, ΔhbpA, and Δhpe strains. To do so, a Spec resistance gene was independently PCR amplified from pRSM2832 using gene-specific mutagenic primer pairs hxuCBA-F2/hxuCBA-R2, hbpA-F2/hbpA-R2, and hpe-F2/hpe-R2 [75]. *E. coli* SW102 cells were prepared for recombineering, separately co-electroporated with pJET1.2-hxuCBA, pJET1.2-hbpA or pJET1.2-hpe (Amp^r) (50 ng), and with each gene-specific mutagenic cassette (Spec^r) (200 ng) [76]. Mutagenized clones containing pJET1.2-hxuCBA::spec, pJET1.2-hbpA::spec and pJET1.2-hpe::spec were selected on LB agar with Amp$_{100}$ and Spec$_{50}$. These plasmids were used as templates to amplify the *hxuCBA*::spec, *hbpA*::spec and *hpe*::spec disruption cassettes with primer pairs hxuCBA-F1/hxuCBA-R1, hbpA-F1/hbpA-R1, and hpe-F1/hpe-R1, respectively. Disruption cassettes were

independently used to transform NTHi375 or Hi RdKW20 by using the MIV method [77]. Transformants were selected on sBHI agar with Erm at 11 μg/ml to obtain ΔsapA and ΔhitBC strains, and on sBHI agar with Spec at 50 μg/ml to obtain ΔhxuCBA, ΔhbpA, and Δhpe strains. All mutants were confirmed by PCR and sequencing. The *sapABCDFZ* and *hbpA*-HI 0854/NTHI1022 are gene clusters containing 6 and 2 genes, respectively. Expression of the *sapBCDFZ* and HI0854/NTHI1022 genes in NTHi375ΔsapA and NTHi375ΔhbpA strains was tested by RT-PCR (see below), being comparable to that found in the wild type (WT) strain (Fig. S1B).

Bacterial growth

Strains grown on chocolate agar were used to generate bacterial suspensions normalized in PBS to OD$_{600}$ = 1. Suspensions were spread on 20 ml BHI agar in the presence of sterile X + V factor disks (Oxoid), and grown during 20 h at 37°C. Growth diameter was measured on at least three independent occasions ($n \geq 3$). Alternatively, normalized bacterial suspensions were diluted to OD$_{600}$ = 0.05 in 2 ml sBHI, and 200 μl aliquots were transferred to individual wells in 96-well microtiter plates (Falcon). Plates were incubated with agitation at 37°C for 6 h in a Multiskan device (ThermoScientific), and OD$_{636}$ was monitored every 15 min. Each growth curve was corrected to its blank values (sBHI). Independently, strains were grown on chocolate agar; biomass was inoculated in 7 ml sBHI and incubated for 8 h at 37°C with shaking (200 r.p.m.). Cultures were centrifuged (10 min, 4000 r.p.m.) and suspensions were normalized to OD$_{600}$ = 1 in PBS. Then, 180 μl of CDMM supplemented with either 50 μM cystine or 50 μM GSSG were transferred to individual wells in 96-well microtiter plates (Sarstedt). Thereafter, 20 μl of the previously prepared bacterial suspensions were added to each well. Plates were incubated in a SpectraMAX 340 microplate reader at 37°C, and OD$_{600}$ was recorded every 30 min for 8 h. In all cases, bacterial growth was monitored in triplicate at least three times ($n \geq 9$).

Heme binding to the bacterial surface

As previously stated [63], strains were grown on chocolate agar, inoculated in 5 ml heme-deficient medium and grown for 8 h, at 37°C with shaking (200 r.p.m.). Next, 100 μl culture aliquots were inoculated into 20 ml sBHI and grown for 16 h under the same conditions. Normalized bacterial suspensions were collected by

centrifugation (10 min, 4000 r.p.m.), washed three times with PBS, and resuspended in 5 ml PBS. For semi-quantitative determination of bacterial heme, 5 ml PBS suspensions were 2-fold serially diluted in PBS, 100 μl aliquots spotted on PVDF membranes, and heme was detected by an enhanced chemiluminescence (ECL) Western Blot detection kit (Pierce).

Co-culture of NTHi3655luxABCDE with heme donors

NTHi3655luxABCDE (recipient) was co-cultured with *H. influenzae* heme donors [63]. Donor strains were grown on chocolate agar, inoculated in 5 ml heme-deficient medium, and grown for 8 h with shaking (200 r.p.m.). Thereafter, 100 μl aliquots of these cultures were added to 20 ml sBHI and grown for 16 h under the same conditions. To generate heme starvation, NTHi3655luxABCDE was grown on chocolate agar, inoculated in 20 ml heme-deficient medium, and grown overnight with shaking (200 r.p.m.). All cultures were then recovered by centrifugation (10 min, 4000 r.p.m.), washed twice in BHI, and resuspended in 10 ml BHI. For co-cultures, appropriate volumes of each suspension (donor and recipient) containing identical number of colony forming units (CFU) were mixed in 5 ml heme-deficient medium generating a starting co-culture with $OD_{600} = 0.1$, to be incubated for 6 h. For recipient controls, similar NTHi3655luxABCDE cultures were prepared and grown in sBHI or heme-deficient medium (positive and negative controls, respectively). Luminescence was monitored every hour for 6 h in a 1,450 MicroBeta TriLux counter (PerkinElmer), using 100 μl bacterial culture aliquots and 96-well black plates (Uniplate®, Whatman). Experiments were performed in triplicates at ≥ 3 independent occassions ($n ≥ 9$).

Bacterial susceptibility to antimicrobials

Antibiotic minimal inhibitory concentrations (MICs) were determined by microdilution using commercial panels (STRHAE2; Sensititre), and interpreted by following the criteria of the Clinical Laboratory Standards Institute (CLSI) [78]. For polymyxin E (PxE), Etests (Biomérieux) on MH-F agar were performed: bacteria were grown on chocolate agar for 8 h, inoculated in 7 ml of heme-deficient medium or sBHI, and grown for 12 h at 37°C, 200 r.p.m. Cultures were centrifuged (10 min, 4000 r.p.m.), suspensions normalized to ~0.5 McFarland (equivalent to $OD_{600} = 0.063$) in saline solution, and used as inoculum on MH-F agar ($n = 2$). To monitor susceptibility to H_2O_2, bacteria grown on chocolate agar for 8 h were inoculated in

7 ml of sBHI, and grown for 12 h at 37°C, 200 r.p.m. Cultures were centrifuged (10 min, 4000 r.p.m.), suspensions were normalized to $OD_{600} = 1$ (~$7×10^8$ CFU/ml) in PBS and plated on sHTM agar on large Petri dishes (20 cm diameter; 80 ml sHTM agar/plate; 1.8 ml suspension/plate). H_2O_2 at 9.8 M (Sigma-Aldrich) was used as stock solution to be diluted in sterile distilled water. Sterile paper disks soaked on 10 μl H_2O_2 containing 25 or 50 μmol were located on the sHTM agar and incubated for 20 h at 37°C. Results are shown as diameter of bacterial growth inhibition (mm) around H_2O_2 disks (means ± SD). Assays were performed at ≥ 3 independent occasions ($n ≥ 3$).

RNA extraction and real-time quantitative PCR (RT-qPCR)

Two to 5 colonies of strains grown on chocolate agar were inoculated in 20 ml sBHI, grown for 11 h, diluted into 40 ml fresh sBHI to $OD_{600} = 0.05$, and grown to $OD_{600} = 0.5$–0.6 (named as conventional sBHI cultures). Alternatively, bacterial biomass was collected from chocolate agar, inoculated in 5 ml heme-deficient medium and grown for 8 h. Next, 100 μl aliquots were inoculated into 20 ml sBHI and grown overnight (37°C, 5% CO_2, 200 r.p.m.). Overnight cultures were collected by centrifugation (10 min, 4000 r.p.m.), washed 3 times in PBS, resuspended in 5 ml PBS, diluted to $OD_{600} = 0.05$ in 40 ml fresh BHI-NAD or sBHI, and grown to $OD_{600} = 0.4$–0.5 [63]. Bacterial total RNA was isolated using TRIzol reagent (Invitrogen), and total RNA quality evaluated using RNA 6,000 Nano LabChips (Agilent 2,100 Bioanalyzer, Santa Clara, CA). All samples had intact 23S and 16S ribosomal RNA bands. Reverse transcription (RT) was performed using 1 μg of RNA by PrimerScript RT Reagent kit (Takara). PCR amplification was performed by using SYBR Premix Ex Taq II (Tli RNaseH Plus) (Takara). Fluorescence was analyzed with AriaMx Real-Time PCR System (Agilent Technologies). The comparative threshold cycle (Ct) method was used to obtain relative quantities of mRNAs that were normalized using 16S ribosomal RNA (*16SrRNA*) as an endogenous control. Primers were designed with Primer3 software (Table S3). All cultures were grown at least three times, and samples were processed with technical triplicates ($n ≥ 3$).

Cell culture and bacterial infection

A549 type II human pneumocytes (ATCC CCL-185) were maintained and seeded as described [79–86]. For infection, PBS-normalized bacterial suspensions

(OD$_{600}$ = 1) were prepared by using NTHi strains grown on chocolate agar. Alternatively, bacteria grown on chocolate agar were inoculated in 7 ml heme-deficient medium or sBHI, and grown for 12 h at 37°C, 200 r.p.m. Cultures were centrifuged (10 min, 4000 r.p. m.), suspensions normalized to OD$_{600}$ = 1 in PBS, and then used as infecting inoculum. A multiplicity of infection (MOI) of ~100:1 was used. To monitor adhesion, cells were infected for 30 min. This assay does not completely exclude a possible internalization of some bacteria, and experimental conditions were previously set to mainly monitor adhesion [84]. For invasion testing, cells were incubated with bacteria for 2 h, washed 3 times with PBS, incubated for 1 h with RPMI 1640 medium containing 10% FCS, 10 mM Hepes, and 200 μg/ml gentamicin. After infection, cells were lysed with PBS-saponin 0.025%, 10-fold diluted and plated on sBHI agar. All infections were performed in triplicates at ≥ 3 independent occasions ($n \geq 9$). Results are expressed as CFU/well.

Secretion of IL-8

Bacteria grown on chocolate agar were collected with PBS, suspensions normalized to OD$_{600}$ = 1 and used for 2 h infection with a MOI of ~100:1. Cells were washed three times with PBS, and incubated for 6 h in RPMI 1640 medium containing 10% FCS, 10 mM Hepes, and 100 μg/ml gentamicin. Supernatants were collected from the wells, cell debris was removed by centrifugation and samples were frozen at −80°C. IL-8 levels in supernatants were measured by ELISA (Abnova KA0115) with sensitivity <2 pg/ml. Infections were performed in duplicate and at least twice (n = 4). Results on IL-8 are expressed in pg/ml.

NTHi mouse lung infection

A mouse model of NTHi lung infection was used as described previously [86]. CD1 female mice were purchased from Charles River Laboratories (France), housed under pathogen-free conditions at the Institute of Agrobiotechnology facilities (registration number 365 ES/31-2016-000002-CR-SU-US), and used at 22–25 g (6–7 weeks). Animal handling and procedures were in accordance with the current European (Directive 2010/63/EU) and National (Real Decreto 53/2013) legislations, following the FELASA and ARRIVE guidelines, with the approval of Universidad Pública de Navarra (UPNa) Animal Experimentation Committee, and in accordance with the Helsinki declaration. Bacteria grown on chocolate agar were recovered in PBS generating normalized suspensions (~5 × 10^9 CFU/ml). Next, 20 μl suspensions

(~1 × 10^8 CFU/mice) were placed at the entrance of the nostrils until complete inhalation, in mice previously anesthetized with ketamine-xylazine (3:1). At 24 or 48 h post-infection (hpi), mice were euthanized using cervical dislocation. Bronchoalveolar lavage fluid (BALF) samples were obtained by perfusion and collection of 0.7 ml of PBS, with help of a sterile 20G (1.1 mm diameter) VialonTM intravenous catheter (Becton-Dickinson) inserted into the trachea. Recovered BALF was serially 10-fold diluted in PBS, and plated in triplicate on sBHI agar to determine the number of viable bacteria. By following standardized published procedures [87], we considered that we could have a minimum of 3.3 CFU in 1 ml of sample without detecting bacteria (limit of detection <3–4 CFU/ml BALF), rendering log$_{10}$ = 0.52. The left lung was individually weighed in sterile bags (Stomacher80, Seward Medical) and homogenized 1:10 (wt/vol) in PBS. Each homogenate was serially 10-fold diluted in PBS and plated in triplicate on sBHI agar to determine the number of CFU per lung. Infections were performed in groups of at least five mice per strain and time point ($n \geq 5$).

Statistical analysis

In all cases, p < 0.05 value was considered statistically significant. Analyses were performed using Prism software, version 7 for Mac (GraphPad Software) statistical package, and are detailed in each figure legend.

Results

Structural basis of heme binding to the HbpA, SapA, PE, and HxuA proteins

First, we investigated the ability of HxuA, HbpA, PE, and SapA to bind heme *in silico* using the HADDOCK (High Ambiguity-Driven Protein DOCKing) server [65,66]. HxuA is part of the heme-hemopexin heme transport system which consists of the HxuC and the two-partner secretion system HxuBA. HxuA is exposed at the cell surface, and its interaction with hemopexin leads to heme release and its capture by HxuC [51–56]. PE is an outer membrane lipoprotein, the dimer of which has been proposed to bind heme [63]; and SapA and HbpA are Cluster C substrate-binding proteins (SBP) that locate at the periplasm and act in concert with the SapBCDFZ and DppBCDF inner membrane ABC transporters, respectively [57,59–62]. Docking results for all four proteins are summarized in Table S4.

Since there are no crystal structures of HbpA and SapA, homology models were constructed based on the crystal

structure of HbpA from *H. parasuis* (*Hp*HbpA) in its glutathione-bound form (PDB code 3M8U) [62] using I-TASSER [67,68]. The sequence identity for the structurally aligned region was 74% and 30% for HbpA and SapA, respectively. Despite the lower sequence identity for SapA, a sequence alignment with HbpA, *Hp*HbpA and the structurally homologous dipeptide-binding protein DppA from *E. coli* (*Ec*DppA) [88] confirmed high sequence similarity (Fig. S2), supporting *Hp*HbpA as a good structural template for SapA as well as HbpA. Ligand binding site residues predicted by COACH [69,70], a ligand-binding prediction server integrated into I-TASSER suite, was used to drive the docking.

For HbpA, the highest scoring docking solution suggests heme binding at a cleft between the N-terminal and C-terminal domains (Figure 2(a–e)), similar to what is seen for binding of glutathione and dipeptide to *Hp*HbpA and *Ec*DppA respectively (Fig. S3A-B). In SapA, heme docks in a similar location but at a different angle due to the presence of a longer loop (residues 140–158, in orange in Figure 2(a,b)). This loop extension is not conserved in

HbpA, *Hp*HbpA and *Ec*DppA, and thus seems to be a unique feature of SapA (Fig. S2). Since the position of this loop must be regarded as speculative due to its absence in the homology modeling template, we removed it from the SapA homology model and repeated the docking experiment. In the absence of the extended loop, the predicted heme binding mode is closer as to what is seen for HbpA, although the site is closer to the protein surface.

Analysis of the heme binding sites using LigPlot[+] [71] shows predicted hydrogen bonds between heme propionates and positively charged side chains or main chain nitrogens in all three cases, as well as the presence of hydrophobic residues lining the pockets and providing van der Waals interaction with the rest of the heme group (Figure 2(c-e) and Fig. S3C-D). Despite the differences in heme binding mode, several residues are common for all three binding sites (colored yellow in Figure 2(c–e)).

For HbpA, the suggested site is supported by what has been previously predicted [89] and corresponds well to a very recent study where heme was docked to *Hp*HbpA, OppA from *H. influenzae* (*Hi*OppA) and NikA from
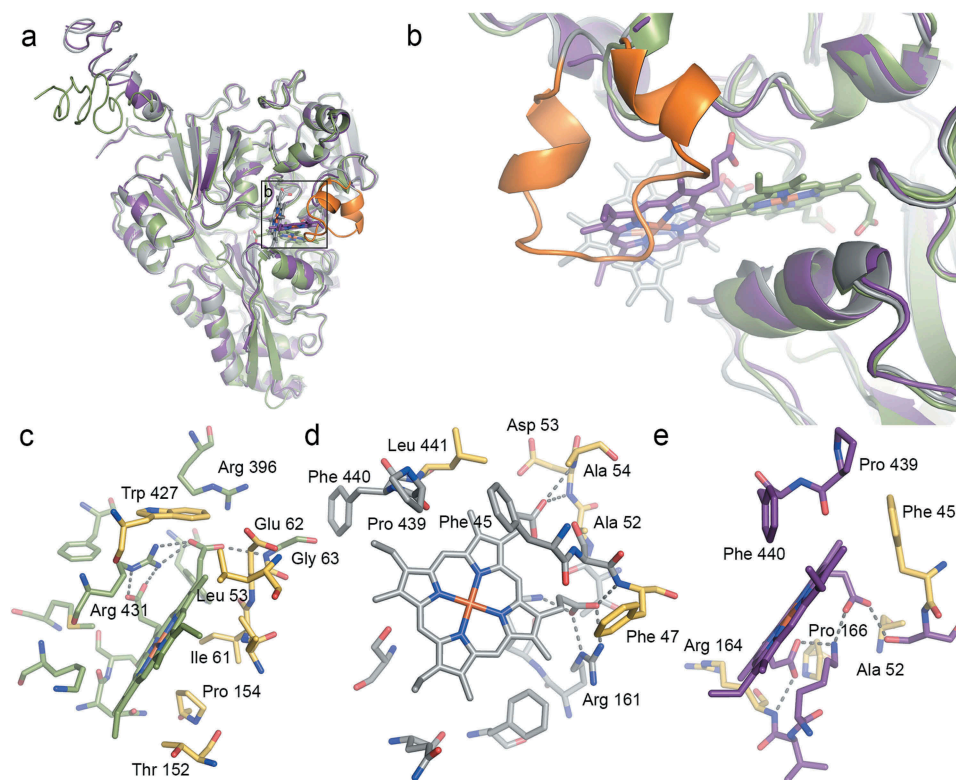
Figure 2. Structural prediction of heme binding to HbpA and SapA. HADDOCK was used to dock heme B to homology models of HbpA (green), full-length SapA (grey) and truncated SapA (purple) in which a non-conserved loop consisting of residues 140–158 has been removed. The truncated residues are colored orange in full-length SapA. **(a)** Overlay of the best scoring docking solutions for HbpA, SapA and truncated SapA. **(b)** Zoom-in on predicted heme binding sites showing how HbpA binds heme deeper into the ligand-binding pocket. In full-length SapA, the non-conserved loop (orange) prevents heme binding into the same pocket whereas in truncated SapA, the pocket is more accessible. **(c-e)** LigPlot[+] analysis of the predicted heme binding site in HbpA **(c)**, full-length SapA **(d)** and truncated SapA **(e)** with residues lining the binding sites in stick representation. Predicted hydrogen bonds are showed as dashed lines. Residues that are common for all three binding sites are colored yellow.

E. coli (*Ec*NikA) [90]. In the latter study, heme was suggested to bind in a site that was distinct but close to the site for other ligands (glutathione for *Hp*HbpA, peptide for *Hi*OppA, and butane-1,2,4-tricarboxylate-chelated nickel for *Ec*NikA) and the ability of bind heme and other ligands simultaneously was demonstrated using surface plasmon resonance. Our docking results reveal a similar scenario, with heme binding close to- but not overlapping with the binding site for glutathione in *Hp*HbpA (Fig. S3).

From the crystal structure of PE, it was suggested that heme could bind in a well-defined pocket formed at the PE dimer interface. Manual docking of heme into this pocket showed that it should be able to accommodate heme but no additional evaluation was performed [63,91]. Here we further explored heme binding to PE by docking heme into the predicted heme-binding pocket. Our results show that heme fits very well with predicted hydrogen bonds formed between heme propionates and polar residues within one of the PE monomers (Asn98, Asn101, and Thr105), as well as van der Waals interactions with hydrophobic residues on both sides of the pocket (Ile65 and Ile96) (Fig. S4A-C).

While HxuC reconstitution in *E. coli* previously showed its ability to act independently as a functional free heme receptor [53], direct heme binding to HxuA has not been demonstrated. Nevertheless, upon examination of the HxuA crystal structure (PDB code 4RM6) [92], we identified a pocket at the HxuA surface, close to the hemopexin binding site, that showed similarities with the predicted heme binding site in HbpA as indicated above, most notably the presence of several positively charged residues that may interact with heme propionates. The ability of this pocket to accommodate a heme molecule was investigated using HADDOCK, resulting in two solutions with similar docking scores (Table S4). As shown in Fig. S4D-E, heme fits well into this pocket, with the two solutions differing by the heme propionates pointing into or out of the pocket. In both solutions, several positively charged residues (Arg and/or Lys) are well positioned to interact with heme propionates via hydrogen bonds.

In summary, our computational studies provide plausible 3D models for how HbpA, SapA, PE, and HxuA interacts with heme.

Expression of NTHi heme binding protein encoding genes and their response to heme availability

*H. influenzae* genes encoding heme-binding proteins are transcribed during acute infection [93]. Multiple heme acquisition systems may counteract NTHi heme auxotrophy and human iron nutritional immunity, but could also lead to redundancy. Based on these assumptions, we asked if the systems under analysis could be interrelated to preserve bacterial fitness or prevent heme overloading toxicity, and if such relationship may occur at the gene expression level.

The NTHi375 strain was employed to independently generate *hxuCBA, sapA, hbpA,* and *hpe* mutants (gene accession numbers NF38_04090/NF38_04085/NF38_04080, NF38_08010/NF38_08015/NF38_08020/NF38_08025/NF38_08030/NF38_08035, NF38_00680, and NF38_04540) (Table 1). Initial characterization of the generated mutants rendered the following features: (i) growth in sBHI, with slightly longer lag phase for the *hxuCBA, hbpA,* and *hpe* mutants than for the WT strain (Fig. S5A). (ii) Aerobic growth on BHI agar around X + V factor disks comparable to that of the WT strain, except for Δ*hxuCBA,* whose growth showed a trend to be lower (NTHi375 WT, 138 ± 17 mm; NTHi375Δ*hxuCBA*, 122 ± 18 mm) (Fig. S5B). (iii) Anaerobic growth on BHI agar around V factor disks, and antibiotic susceptibility patterns (Table S5) similar to the WT strain. (iv) Inactivation of heme acquisition systems could modify bacterial iron levels and subsequently, iron reactivity with H_2O_2 via the Fenton reaction. To prove this phenomenon, inactivation of the *sapA* and *hbpA* genes increased growth inhibition around paper disks soaked with H_2O_2 25 and 50 μmol compared to the WT strain (Fig. S5C).

NTHi375 WT and mutant strains were used to determine the expression of the *hxuA, sapA, hbpA,* and *hpe* genes. First, conventional sBHI cultures were employed. The *hbpA* gene was highly expressed in all cases, with higher expression than that of the *hxuA, sapA,* and *hpe* genes. Inactivation of the *hxuA, sapA,* and *hpe* genes did not alter *hbpA* gene expression. However, expression of the *hxuA, sapA,* and *hpe* genes showed a consistent trend to be higher in the mutants than in the WT strain, being significant for the *hxuA* and *hpe* genes when comparing their expression in the WT and NTHi375Δ*hbpA* strains (Figure 3(a)).

Bacteria sense heme as means to alert pathogens upon contact with vertebrate tissues, thus modulating expression of systems involved in heme acquisition and metabolism [29,94]. Expression of genes encoding most heme uptake systems increases when iron or heme are restricted [95,96]. We next asked if gene expression responsive to heme availability occurs in a coordinated manner. NTHi375 WT and mutant strains were grown in heme-deficient medium or in sBHI for RNA purification and qRT-PCR analyses. In NTHi375 WT, Δ*hbpA,* and Δ*hpe* strains, expression
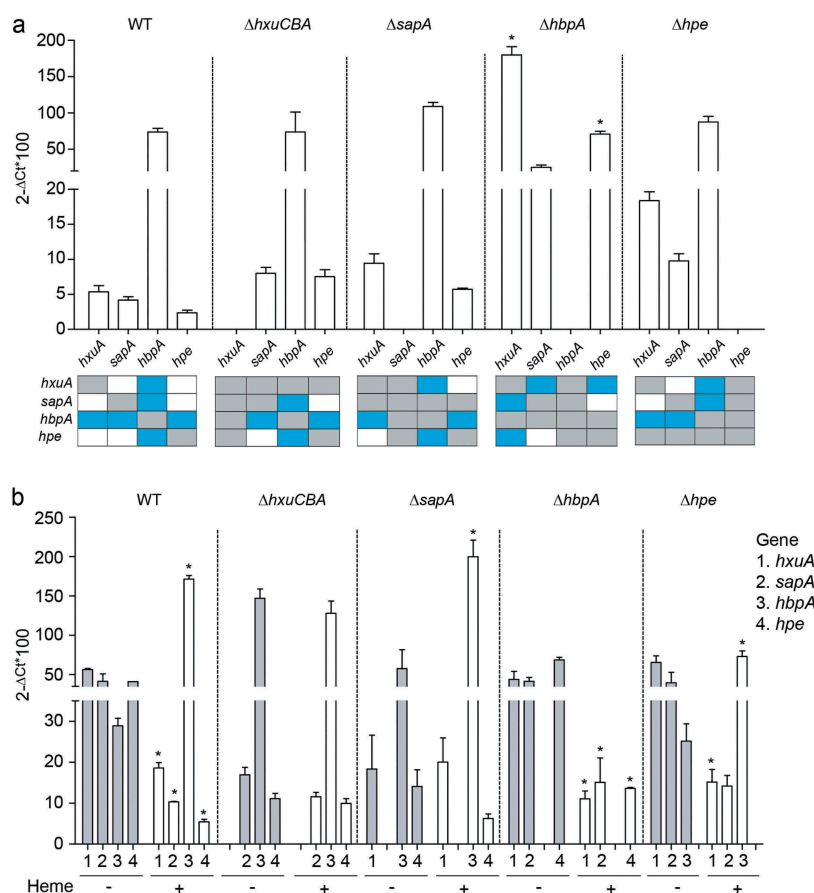
Figure 3. Expression of NTHi heme acquisition systems. (a) Expression of the *hxuA, sapA, hbpA* and *hpe* genes in NTHi375 WT, Δ*hxuCBA*, Δ*sapA*, Δ*hbpA*, and Δ*hpe* strains grown in sBHI. Expression of the *hbpA* gene was higher than that of *hxuA, sapA,* and *hpe* (WT strain, higher expression of *hbpA* than that of *hxuA* (p < 0.05), *sapA* and *hpe* (p < 0.01); NTHi375Δ*hxuCBA*, higher expression of *hbpA* than that of *sapA* and *hpe* (p < 0.0005); NTHi375Δ*sapA*, higher expression of *hbpA* than that of *hxuA* and *hpe* (p < 0.0005); NTHi375Δ*hpe*, higher expression of *hbpA* than that of *hxuA* (p < 0.05) and *sapA* (p < 0.0005)). Expression of the *hxuA* and *hpe* genes was higher in NTHi375Δ*hbpA* than in the WT strain (p < 0.0001 and p < 0.01, respectively). Bottom panel: schematic representation of each gene expression compared to each other, in the WT and mutant strains. Color code: blue, statistically significant differences; gray, not determined; white, no significant differences. Data are shown as mean ± SEM. Statistical comparisons of the means were performed with two-way ANOVA (Tukey´s multiple comparisons test). **(b)** Gene expression and heme sensing. In NTHi375 WT, Δ*hbpA* and Δ*hpe* strains, *hxuA, sapA,* and *hpe* gene expression was higher in heme-restricted medium than in sBHI (WT: *hxuA* (p < 0.001), *sapA* (p < 0.01), *hpe* (p < 0.001); NTHi375Δ*hbpA*: *hxuA* (p < 0.01), *sapA* (p < 0.05), *hpe* (p < 0.0001); NTHi375Δ*hpe*, *hxuA*, p < 0.05). In NTHi375 WT, Δ*sapA* and Δ*hpe* strains, expression of *hbpA* was lower upon heme depletion (WT, p < 0.0001; NTHi375Δ*sapA*, (p < 0.001); NTHi375Δ*hpe*, p < 0.05). Data are shown as mean ± SEM. Statistical comparisons of the means were performed with two-way ANOVA (Sidak´s multiple comparisons test).

of the *hxuA, sapA,* and *hpe* (the latter in WT and Δ*hbpA* strains) genes was higher in heme-restricted medium than in sBHI. In NTHi375 WT, Δ*sapA*, and Δ*hpe* strains, expression of the *hbpA* gene was lower upon heme depletion. Lastly, *hxuCBA* gene inactivation seemed to hamper the effect of heme availability on gene expression (Figure 3(b)).

Overall, these results support the notion that NTHi heme acquisition machinery may act in a coordinated manner, where HbpA seems to play a prominent role, likely followed by PE, and HxuCBA and SapABCDFZ participate in heme sensing, in turn having an impact on the expression of other uptake systems.

SapA, HbpA, and HxuA participate in heme donation to heme-starved NTHi bacterial cells

PE functions as a heme reservoir at the bacterial surface, which can be donated to other *H. influenzae* bacterial cells starved of heme [63]. We asked if this PE trait could be extended to the other heme-binding proteins. Monitoring heme donation as a means of luminescent emission requires co-culturing a recipient luminescent strain starved of heme and a donor strain cultured in the presence of heme [63]. Unexpectedly, NTHi375 was a poor heme donor, rendering very limited recipient growth (Fig. S6A); in contrast, *H. influenzae* reference strain RdKW20, which also contains the heme acquisition systems under

study (*hxuCBA*, HI0262_HI0263_HI0264; *sapABCDFZ*, HI1638_HI1639_HI1640_HI1641_HI1642_HI1643; *hbpA*, HI0853) [97], donates heme at a significantly higher rate (Figure 4(a)). While comparing NTHi375 and RdKW20 donor strains, we found that the *hbpA* gene expression was significantly higher in the latter (Fig. S6B). This limitation by NTHi375 led us to perform gene inactivation in RdKW20 to analyze heme storage and inter-bacterial donation. The growth of the generated mutants in sBHI was comparable to that of the WT strain (Fig. S6C). We assessed the use of heme derived from SapA, HbpA, and

HxuCBA by setting up co-cultures of NTH i3655*luxABCDE* starved of heme with RdKW20 WT or mutant strains cultured with heme. NTHi3655*luxABCDE* grew better when incubated with RdKW20 WT as compared to co-culture with RdKW20Δ*sapA*, RdKW20Δ*hbpA*, or RdKW20Δ*hxuCBA* mutants (Figure 4(a)). We next asked if heme interbacterial donation relates to its binding. To do so, we employed the free iron-binding system HitABC, in which HitA is a periplasmic protein that binds free iron linked to the HitBC transporter located at the inner membrane [98–101]. Inactivation of the *hitABC*
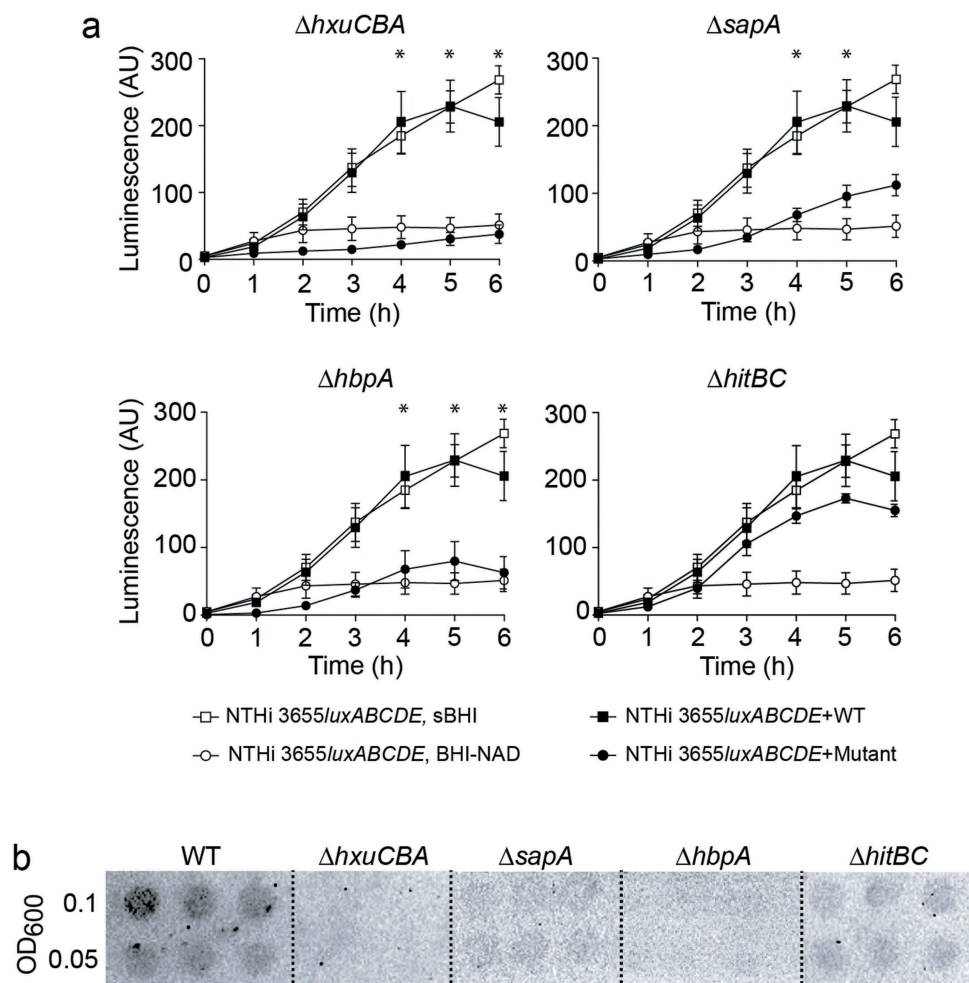
Figure 4. **HxuCBA, SapA and HbpA participate in heme inter-bacterial donation. (a)** Heme-starved NTHi 3655*luxABCDE* was used as a heme-recipient strain. Heme donation allowed recipient´s growth, measured as a means of luminescence. NTHi 3655*luxABCDE* co-culture with Hi RdKW20 WT rendered significant recipient growth, comparable to that of NTHi 3655*luxABCDE* grown in sBHI; in contrast, NTHi 3655*luxABCDE* co-culture with Δ*hxuCBA*, Δ*sapA* or Δ*hbpA*, did not promote recipient strain growth at the same extent (see growth time points 4, 5 and 6 h). HitABC does not contribute to surface-bound heme inter-bacterial donation. NTHi 3655*luxABCDE* co-culture with both Hi RdKW20 WT and Δ*hitBC* rendered significant recipient growth. White symbols, controls showing recipient strain growth in sBHI (square) or BHI-NAD (circle). Black symbols, recipient strain growth when co-cultured with WT (square) or mutant (circle) strains. *Indicates significant differences when comparing luminescence upon recipient co-culture with WT (square) or mutant (circle) strains. Data are shown as luminescence arbitrary units (AU) and represent mean ± SEM values. Statistical comparisons of the means were performed with two-way ANOVA (Bonferroni multiple comparisons test). **(b)** Semi-quantitative measure of heme binding on the surface of Hi RdKW20 WT and mutant strains. Normalized bacterial suspensions were 2-fold serially diluted (OD$_{600}$ = 0.1 and 0.05) and spotted on a PVDF filter. ECL was used for heme detection. Blots are representative images of at least three independent experiments.

system was performed in RdKW20 (HI0097_HI0098_HI0099). Growth of the generated mutant in sBHI was comparable to that of the WT strain (Fig. S6C). When co-culturing NTHi3655luxABCDE starved of heme with RdKW20ΔhitBC cultured with heme, NTHi3655luxABCDE growth was comparable to that obtained by co-culturing with the WT strain (Figure 4(a)), excluding participation of this free iron transport system in heme donation [98,99,101]. Lastly, deficiency in heme inter-bacterial donation may relate to lower heme binding at the bacterial surface. In fact, more heme was bound to WT than to the *hxuCBA, sapA,* and *hbpA* mutants. Unexpectedly, RdKW20ΔhitBC displayed a slight reduction in heme binding, but to a lower extent than that by the ΔhxuCBA, ΔsapA, and ΔhbpA strains (Figure 4(b)).
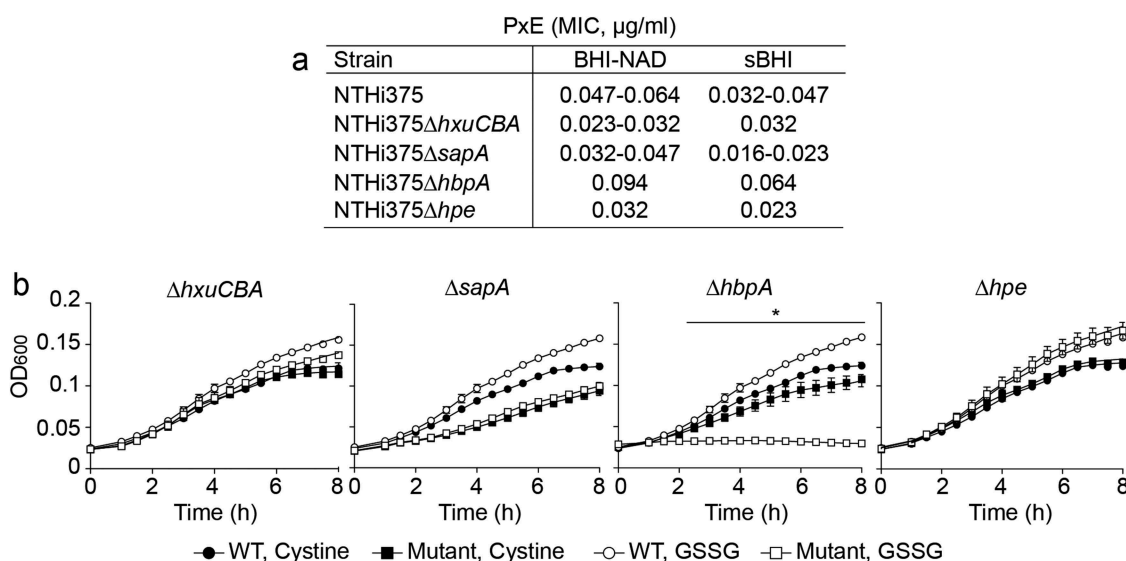
Overall, these results suggest that heme binding may work as a storage pool for heme to be shared between *H. influenzae* bacterial cells during shortage. This ability which was previously observed for the outer membrane lipoprotein PE [63] is now extended to HxuCBA, SapA, and HbpA.

Moonlighting features of H. influenzae heme-binding systems

Besides heme binding, SapA is required for NTHi resistance to antimicrobial peptides (AMP) and potassium acquisition, HbpA is essential for glutathione import, and PE binds extracellular matrix proteins [62,91,102–106]. To get further insight on the multi-functionality of the heme acquisition systems under study, we tested their contribution to NTHi resistance to polymyxin E (PxE) as a representative AMP. Inactivation of the *hxuCBA, sapA,* and *hpe* genes rendered reduced MIC for this AMP; conversely, *hbpA* gene inactivation increased PxE MIC. Mutant strains showed comparable relative phenotypes when grown in heme-deficient medium or in sBHI (Figure 5(a)). Moreover, we tested their contribution to glutathione import, a vital L-cysteine-containing tripeptide mediating protection against oxidative, xenobiotic, and metal iron stresses [107,108]. *H. influenzae* is a cysteine and glutathione auxotroph, and imports both molecules. Exogenous cysteine and glutathione, and their oxidized forms cystine and glutathione disulfide (GSSG), sustain *H. influenzae* growth comparably [73]. NTHi375 WT and mutant strains were inoculated in CDMM supplemented with cystine or GSSG. CDMM supplemented with cystine sustained bacterial growth in all cases. In contrast, CDMM supplemented with GSSG did not sustain NTHi375ΔhbpA growth. NTHi375ΔsapA growth was lower than that of the WT strain, but comparable in CDMM supplemented with cystine or GSSG (Figure 5(b)).

In conclusion, besides their common role in heme binding, HxuCBA, SapA, and PE also account for AMP resistance, and HbpA accounts for gluthatione import.

PxE (MIC, μg/ml)		
Strain	BHI-NAD	sBHI
NTHi375	0.047-0.064	0.032-0.047
NTHi375ΔhxuCBA	0.023-0.032	0.032
NTHi375ΔsapA	0.032-0.047	0.016-0.023
NTHi375ΔhbpA	0.094	0.064
NTHi375Δhpe	0.032	0.023

Figure 5. Moonlighting features of NTHi heme acquisition systems. (a) HxuCBA, SapABCDFZ and PE are involved in NTHi resistance to PxE. MIC for PxE was shown to be lower for ΔhxuCBA, ΔsapA and Δhpe mutants than for the WT strain. Inactivation of the *hbpA* gene rendered higher MIC for PxE. Bacterial inocula were prepared on heme-deficient or sBHI media. **(b)** HbpA, but not HxuCBA, SapABCDFZ or PE, participates in glutathione import by NTHi. Bacteria were grown in CDMM supplemented with cystine or GSSG. CDMM+cystine sustained bacterial growth in all cases. NTHi375ΔhbpA growth was lower in CDMM+GSSG than in CDMM+cystine (at 2.5 h, p < 0.05; 3 h, p < 0.001; from 3.5 to 8 h p < 0.0001). Data are shown as mean ± SEM. Statistical comparisons of the means were performed using two-way ANOVA (Tukey´s multiple comparisons test).

NTHi heme acquisition systems contribute to host airways-pathogen interplay

Production of dedicated heme scavenging machinery may also relate to successful bacterial-host interplay [1,6]. We asked whether inactivation of the systems under analysis alters NTHi interplay with A549 type II human pneumocytes. Epithelial invasion by NTHi375Δ*hxuCBA*, NTHi375Δ*sapA*, NTHi375Δ*hbpA,* and NTHi375Δ*hpe* was lower than that observed for the WT strain (Figure 6 (a)). All strains stimulated epithelial IL-8 secretion, but such inflammatory response was lower for NTHi375Δ*hxuCBA*, NTHi375Δ*sapA,* and NTHi375Δ*hpe* than for the WT strain (Fig. S7A). We next assessed if heme availability modulates the NTHi-host cell interplay by growing NTHi375 WT and mutant strains in heme-deficient medium or sBHI before infection. Epithelial invasion for the mutants was lower than for the WT strain in all cases. Moreover, BHI-NAD rendered lower invasion when compared to that of bacteria grown in sBHI. However, while comparing invasion by BHI-NAD to that of sBHI grown bacteria, the ratio of increased invasion upon growth in sBHI was higher for the mutants (for NTHi375Δ*hxuCBA*, 17.5-fold; for NTHi375Δ*sapA*, 42-fold; for NTHi375Δ*hbpA*, 22.3-fold; for NTHi375Δ*hpe*, 18.5-fold) than for the WT strain, 4.5-fold (Figure 6(b)). At a lower extent, similar observations were obtained when assessing epithelial adhesion (Fig. S7B). Last, we used an *in vivo* mouse respiratory infection model system [79–81,85,86]. At 24 hpi, NTHi375Δ*hxuCBA* lung and BALF bacterial numbers were lower than those recovered for the WT strain (Figure 6(c), left panels). At 48 hpi, the four tested mutants rendered numbers lower than those of the WT strain in both lung and BALF samples (Figure 6(c), right panels).

In summary, these results support that, under the conditions tested, inactivation of the HxuCBA, SapABCDFZ, HbpA, and PE systems impairs airway infection by NTHi, and that bacterial heme binding may facilitate its interplay with host epithelial cells.

Discussion

Microorganisms have evolved or acquired a variety of specialized iron uptake systems to overcome its environmental limitation and take up iron from extracellular sources, including during infection [109]. For many Gram negative bacteria (including uropathogenic *E. coli, Pseudomonas aeruginosa, Neisseria meningitidis, Acinetobacter baumannii*), Gram positive species (*Staphylococcus aureus*), and fungal pathogens (*Candida albicans, Cryptococcus neoformans*), heme provides the potential for a rich source of iron [110].

Here, we tackled the *H. influenzae* case, a human host-restricted opportunistic pathogen colonizing the lower airways of patients who undergo iron homeostasis unbalancing (i.e. COPD), and that requires exogenous heme for aerobic respiration, lacks siderophore production, and presents a panel of heme acquisition systems. In this study, differential contribution of HxuCBA, SapA, HbpA, and PE systems to NTHi respiratory infection was evaluated.

The proteins HxuA, SapA, HbpA, and PE share the ability to bind heme. We provide evidence for heme binding to SapA and HbpA Cluster C substrate-binding proteins (SBP) as well as information on the shared predicted structural basis of such binding. In fact, one striking feature of the Cluster C family is that members play dual roles in nutrient uptake, importing their canonical substrates and heme. In NTHi, four Cluster C proteins with capability to bind heme have been identified: HbpA, SapA, and OppA, which bind hydrophobic oligopeptides, and NTHI0310 with an unknown canonical substrate specificity. These proteins present overlapping functionality and multisubstrate specificity [90]. This may not be exclusive to NTHi given that the *E. coli* Cluster C nickel SBP NikA binds heme and plays a role as a heme chaperone in the periplasm [111]. Regarding HxuA, it should be stressed that our structural analyses may support heme binding, together with the experimental evidence presented in Figure 4 whereas previous data suggests heme binding to HxuC, when expressed together with the NTHi TonB complex in an *E. coli* heterologous host [53]. The mode of heme binding to PE has been predicted previously [63], and our docking analysis supports this and gives further details about the residues involved.

Apart from the requirement for aerobic respiration, bound heme may also be stored at the bacterial surface or donated to neighboring heme-starved bacterial cells, by contribution of these systems. SapA and HbpA are predicted periplasmic proteins, and may need to be coupled to other currently unknown bacterial systems for effective heme uptake and donation. Moreover, we should not exclude that deficiency in heme donation by the *sapA* and *hbpA* mutants could also be an indirect effect. We acknowledge that using RdKW20 mutants to assess heme inter-bacterial donation may be a potential limitation given our use of the NTHi375 strain in the entire study, however, that it should be noted that RdKW20 rendered a useful tool to generate this specific information. Expression of the *hxuA, sapA,* and *hpe* genes was comparable between NTHi375 and RdKW20 WT strains, and was in parallel to expression to the same level of the *hitB, tonB, tbpA,* and *dppB*
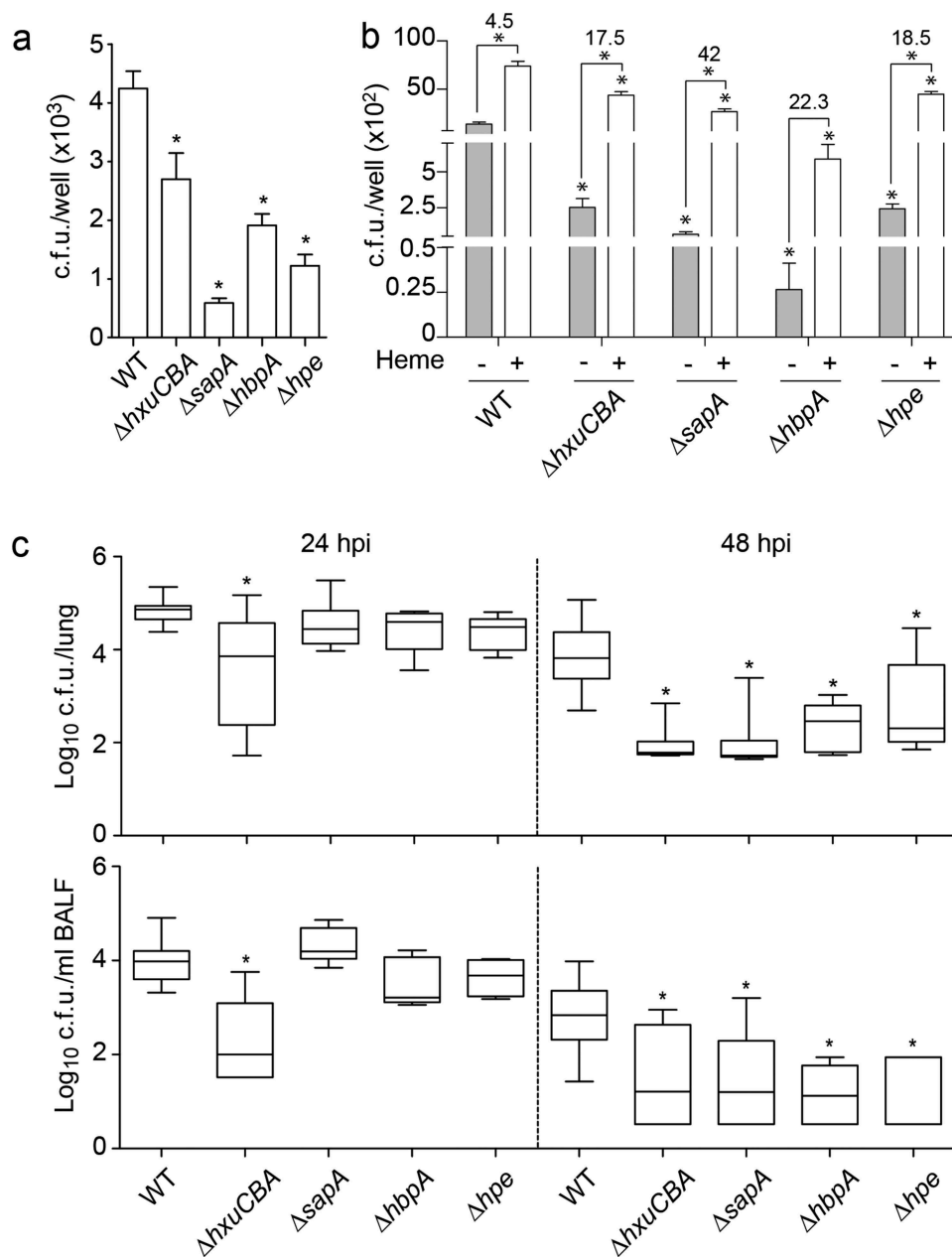
Figure 6. NTHi heme acquisition systems contribute to the host airway-pathogen interplay. (a) Effect of heme uptake inactivation in NTHi interplay with cultured cells. A549 cells were used to quantify invasion by NTHi375 WT, ΔhxuCBA, ΔsapA, ΔhbpA and Δhpe strains. Gene inactivation rendered significantly lower entry into A549 cells than that shown by the WT strain (ΔhxuCBA, $p < 0.05$; ΔsapA and Δhpe, $p < 0.0001$; ΔhbpA, $p < 0.001$). Mean ± SEM values are shown, statistical comparisons of the means were performed using one-way ANOVA (Dunnett's multiple comparison test). **(b)** Inactivation of heme-binding systems lowers NTHi interaction with airway epithelial cells in a heme-dependent manner. BHI-NAD (gray bars) and sBHI (white bars) led to decreased A549 invasion rates for the mutants, compared to that of the WT strain ($p < 0.0001$). Bacterial growth in sBHI increased invasion rates, compared to BHI-NAD (for WT, ΔhxuCBA, ΔsapA and Δhpe, $p < 0.0001$). Top numbers indicate invasion fold increase for each strain upon growth in sBHI compared to BHI-NAD. Mean ± SEM values are shown, statistical comparisons of the means were performed using two-way ANOVA (Sidak's multiple comparison test). **(c)** Effect of heme uptake inactivation in NTHi pulmonary infection. CD1 mice were intranasally infected with WT and mutant strains, euthanized at 24 and 48 hpi, and bacterial loads quantified. Results are reported as log_{10} CFU/lung and log_{10} CFU/ml BALF in upper and lower panels, respectively, and represented as box plot graphs (lines inside boxes represent median values). Statistical comparisons were performed using one-way ANOVA (Dunnett's multiple comparison test). In the lungs, NTHi375ΔhxuCBA showed significantly lower loads at 24 hpi (ΔhxuCBA, $p < 0.0005$), and all mutants showed significantly lower loads at 48 hpi (ΔhxuCBA, ΔsapA, $p < 0.0001$; ΔhbpA, $p < 0.001$; Δhpe, $p < 0.05$) than those shown by the WT strain. In BALF samples, NTHi375ΔhxuCBA showed significantly lower loads at 24 hpi ($p < 0.0001$), and all mutants showed significantly lower loads at 48 hpi (ΔhxuCBA, $p < 0.05$; Δhpe, $p < 0.01$; ΔsapA and ΔhbpA $p < 0.005$) than those shown by the WT strain.

heme-iron uptake related genes; only *hbpA* gene expression was higher in RdKW20 than in NTHi375 strain, which could have an effect on the observed differences between strain backgrounds (Fig. S6B). Although the precise reason for limited heme interbacterial donation by NTHi375 is unknown, we provide several evidences suggesting heme binding at this bacterial surface: heme availability increased alveolar epithelial infection by NTHi375, and also increased NTHi375 susceptibility to PxE (more clearly shown for WT, *sapA, hxuCBA,* and *hpe* mutant strains) supporting the notion of AMP and heme competition for binding to SapA [58], HxuA or PE.

When tackling a possible relationship among heme uptake systems at the gene expression level, a prominent role for HbpA was observed, based on its high expression and on the effect of its inactivation on the expression of the *hxuA, sapA,* and *hpe* genes, suggesting HbpA contribution to down-regulating the activity of other heme piracy systems. However, HbpA does not seem to participate in heme sensing. In fact, in NTHi375 WT, Δ*hbpA,* and Δ*hpe* strains, expression of the *hxuA, sapA,* and *hpe* genes was higher in heme-restricted than in sBHI medium, supporting the notion that the expression of those genes is up-regulated upon heme restriction in a HbpA- and PE-independent manner. Conversely, in NTHi375 WT, Δ*sapA,* and Δ*hpe* strains, expression of the *hbpA* gene was lower upon heme depletion, suggesting *hbpA* gene expression being down-regulated upon heme restriction in a SapABCDFZ- and PE-independent manner. For unknown reasons, we noticed that expression of the *hxuA, sapA,* and *hpe* genes in NTHi375Δ*hbpA* was higher when conventionally grown in sBHI (Figure 3 (a)) than in sBHI while assessing the effect of heme availability (Figure 3(b)). We acknowledge that BHI is a medium with non-defined composition that could render reproducibility issues, and emphasize the importance of preserving the use of exactly the same product in each experimental design, as performed in this study. Although to a lesser extent for HxuCBA, SapABCDFZ, and PE, heme acquisition interlinks may contribute to regulating the expression of the different systems, altogether compatible with the notion of a coordinated heme uptake network preventing toxicity by heme excess.

Notably, the heme uptake systems studied present moonlighting features (summarized in Figure 7). We highlight a relationship between NTHi heme acquisition and AMPs. In addition to the already reported involvement of SapABCDFZ in resistance to AMPs [102,103,112], HxuCBA and PE also seem to subvert these elements of the human soluble innate immunity. This was not the case for NTHi375Δ*hbpA*, which could be linked to the observed higher expression levels of the *hxuA, sapA,* and *hpe* genes
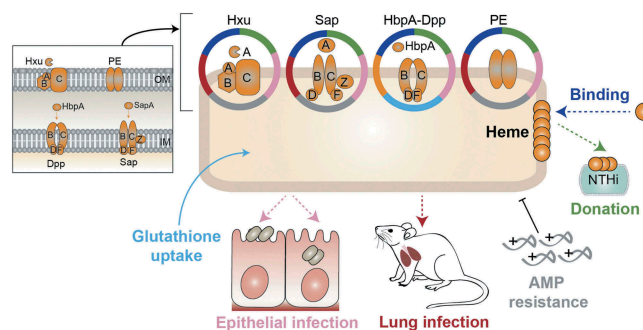
Figure 7. Schematic model showing moonlighting patterns by HxuCBA, SapABCDFZ, HbpA-DppBCDF and PE heme acquisition systems.

upon *hbpA* gene inactivation. Monitoring AMP resistance was motivated by an earlier study where we conducted a genomic analysis of three NTHi clonal isolates serially collected from a bronchiectasis patient, which showed increasing AMP resistance and carried amino acid substitutions in SapABCDFZ and HxuCBA [113]. Based on that and current observations, molecular crosstalk between NTHi heme acquisition and AMP resistance will be addressed in further studies. We also asked if glutathione import could add to protein multi-functionality. This was only the case for HbpA, in line with previous observations [62].

The use of cultured airway epithelia and murine pulmonary infection model systems revealed a significant involvement for heme binding systems in the bacterial-host interplay. Data obtained for NTHi375Δ*hpe* support the role of PE as an adhesin [105,106]. In contrast, the *sapA* gene inactivation has been shown to increase bacterial invasiveness [104], which could relate to the use of non-polarized (this study) *versus* polarized epithelial cells grown at an air-liquid interface [104]. On the other hand, increased invasion by the WT NTHi strain when pregrown in sBHI, and heme rescue of *hxuCBA, sapA, hbpA,* and *hpe* mutant deficiencies upon epithelial infection, could relate to pathogen subversion of host cell heme receptors such as heme uptake proteins HCP1 and HRG1 by using bound heme as a ligand. Our results somehow differ from those shown by transient iron deprived bacteria developing intracellular bacterial communities [64,114], which could relate to the use of different host cell lines, bacterial strains, or growth conditions. A role for HbpA and HxuCBA in causing bacteremia has been shown in a rat model of invasive disease [55,60], and for SapABCDFZ in a chinchilla model of otitis media (SapA, SapF [103,112,115]) and a mouse model of lung infection (SapF [116]). By using a mouse model of lung infection, we expanded previous observations on HbpA, HxuCBA and SapABCDFZ, and provided new roles for the PE heme-acquisition system *in vivo*.

In conclusion, the "iron-loving" bacterial species *H. influenzae* has evolved redundant mechanisms to obtain heme from the human host, and several of them present specific moonlighting properties. We also began elucidating the complex regulatory networks used by NTHi to adapt to the host airways. In general terms, pharmacological modification of host heme-iron metabolism and/or acquisition may hold a key to develop novel strategies to treat or prevent infection. Iron chelators with improved pharmacokinetic properties may become important antimicrobials, and heme-iron transporters and acquisition pathways attractive targets for the development of new treatments to fight infections in an era of increasing burden of antibiotic resistance.

Acknowledgments

Disclosure statement

No potential conflict of interest was reported by the authors.

Funding

ORCID

Tamim Al-Jubair http://orcid.org/0000-0001-6954-5293
Ariadna Fernández-Calvet http://orcid.org/0000-0002-3340-703X
Kristian Riesbeck http://orcid.org/0000-0001-6274-6965

References

[1] Ali MK, Kim RY, Karim R, et al. Role of iron in the pathogenesis of respiratory disease. Int J Biochem Cell Biol. 2017 Jul;88:181–195. PubMed PMID: 28495571.

[2] Ghio AJ. Disruption of iron homeostasis and lung disease. Biochim Biophys Acta. 2009 Jul;1790 (7):731–739. PubMed PMID: 19100311.

[3] Barber MF, Elde NC. Buried treasure: evolutionary perspectives on microbial iron piracy. Trends Genet. 2015 Nov;31(11):627–636. PubMed PMID: 26431675.

[4] Krewulak KD, Vogel HJ. Structural biology of bacterial iron uptake. Biochim Biophys Acta. 2008 Sep;1778 (9):1781–1804. PubMed PMID: 17916327.

[5] Choby JE, Skaar EP. Heme synthesis and acquisition in bacterial pathogens. J Mol Biol. 2016 Aug 28;428 (17):3408–3428. PubMed PMID: 270192980.

[6] Cassat JE, Skaar EP. Iron in infection and immunity. Cell Host Microbe. 2013 May 15;13(5):509–519. PubMed PMID: 23684303.

[7] Hood MI, Skaar EP. Nutritional immunity: transition metals at the pathogen-host interface. Nat Rev Microbiol. 2012 Jul 16;10(8):525–537. PubMed PMID: 22796883.

[8] Runyen-Janecky LJ. Role and regulation of heme iron acquisition in gram-negative pathogens. Front Cell Infect Microbiol. 2013;3:55. PubMed PMID: 24116354.

[9] Gammella E, Buratti P, Cairo G, et al. Macrophages: central regulators of iron balance. Metallomics. 2014 Aug;6(8):1336–1345. PubMed PMID: 24905850.

[10] Ganz T. Macrophages and systemic iron homeostasis. PubMed PMID: 22441209 J Innate Immun. 2012;4 (5–6):446–453.

[11] Ghio AJ, Turi JL, Yang F, et al. Iron homeostasis in the lung. Biol Res. 2006;39(1):67–77. PubMed PMID: 16629166.

[12] Cloonan SM, Mumby S, Adcock IM, et al. The "iron"-y of iron overload and iron deficiency in chronic obstructive pulmonary disease. Am J Respir Crit Care Med. 2017 Nov 1;196(9):1103–1112. PubMed PMID: 28410559.

[13] Ghio AJ, Hilborn ED, Stonehuerner JG, et al. Particulate matter in cigarette smoke alters iron homeostasis to produce a biological effect. Am J Respir Crit Care Med. 2008 Dec 1;178 (11):1130–1138. PubMed PMID: 18723436.

[14] Ghio AJ, Stonehuerner JG, Richards JH, et al. Iron homeostasis and oxidative stress in idiopathic pulmonary alveolar proteinosis: a case-control study. Respir Res. 2008 Jan 23;9:10. PubMed PMID: 18215276.

[15] Gozzelino R, Arosio P. Iron homeostasis in health and disease. Int J Mol Sci. 2016 Jan 20;17(1):130. PubMed PMID: 26805813.

[16] Berg K, Wright JL. The pathology of chronic obstructive pulmonary disease: progress in the 20th and 21st centuries. Arch Pathol Lab Med. 2016 Dec;140 (12):1423–1428. PubMed PMID: 27922768.

[17] Wong J, Magun BE, Wood LJ. Lung inflammation caused by inhaled toxicants: a review. Int J Chron Obstruct Pulmon Dis. 2016;11:1391–1401. PubMed PMID: 27382275.

[18] Nelson ME, O'Brien-Ladner AR, Wesselius LJ. Regional variation in iron and iron-binding proteins within the lungs of smokers. Am J Respir Crit Care Med. 1996 Apr;153(4 Pt 1):1353–1358. PubMed PMID: 8616566.

[19] O'Brien-Ladner AR, Nelson SR, Murphy WJ, et al. Iron is a regulatory component of human IL-1b production. Support for regional variability in the lung. Am J Respir Cell Mol Biol. 2000 Jul;23(1):112–119. PubMed PMID: 10873160.

[20] Thompson AB, Bohling T, Heires A, et al. Lower respiratory tract iron burden is increased in association with cigarette smoking. J Lab Clin Med. 1991 Jun;117(6):493–499. PubMed PMID: 2045717.

[21] Chappell SL, Daly L, Lotya J, et al. The role of IREB2 and transforming growth factor b-1 genetic variants in COPD: a replication case-control study. BMC Med Genet. 2011 Feb 14;12:24. PubMed PMID: 21320324.

[22] Cloonan SM, Glass K, Laucho-Contreras ME, et al. Mitochondrial iron chelation ameliorates cigarette smoke-induced bronchitis and emphysema in mice. Nat Med. 2016 Feb;22(2):163–174. PubMed PMID: 26752519.

[23] DeMeo DL, Mariani T, Bhattacharya S, et al. Integration of genomic and genetic approaches implicates IREB2 as a COPD susceptibility gene. Am J Hum Genet. 2009 Oct;85(4):493–502. PubMed PMID: 19800047.

[24] Eagan TM, Damas JK, Ueland T, et al. Neutrophil gelatinase-associated lipocalin: a biomarker in COPD. Chest. 2010 Oct;138(4):888–895. PubMed PMID: 20495108.

[25] Engstrom G, Segelstorm N, Ekberg-Aronsson M, et al. Plasma markers of inflammation and incidence of hospitalisations for COPD: results from a population-based cohort study. Thorax. 2009 Mar;64 (3):211–215. PubMed PMID: 18988660.

[26] Philippot Q, Deslee G, Adair-Kirk TL, et al. Increased iron sequestration in alveolar macrophages in chronic obstructive pulmonary disease. PLoS One. 2014;9(5): e96285. PubMed PMID: 24789352.

[27] Pillai SG, Ge D, Zhu G, et al. A genome-wide association study in chronic obstructive pulmonary disease (COPD): identification of two major susceptibility loci. PLoS Genet. 2009 Mar;5(3):e1000421. PubMed PMID: 19300482.

[28] Tandara L, Grubisic TZ, Ivan G, et al. Systemic inflammation up-regulates serum hepcidin in exacerbations and stabile chronic obstructive pulmonary disease. Clin Biochem. 2015 Dec;48(18):1252–1257. PubMed PMID: 26164540.

[29] Skaar EP. The battle for iron between bacterial pathogens and their vertebrate hosts. PLoS Pathog. 2010 Aug 12;6(8):e1000949. PubMed PMID: 20711357.

[30] Soares MP, Weiss G. The iron age of host-microbe interactions. EMBO Rep. 2015 Nov;16(11):1482–1500. PubMed PMID: 26474900.

[31] Ahearn CP, Gallo MC, Murphy TF. Insights on persistent airway infection by non-typeable Haemophilus influenzae in chronic obstructive pulmonary disease. Pathog Dis. 2017 Jun 1;75(4). PubMed PMID: 28449098. DOI:10.1093/femspd/ftx042.

[32] Bandi V, Apicella MA, Mason E, et al. Nontypeable Haemophilus influenzae in the lower respiratory tract of patients with chronic bronchitis. Am J Respir Crit Care Med. 2001 Dec 1;164(11):2114–2119. PubMed PMID: 11739144.

[33] Finney LJ, Ritchie A, Pollard E, et al. Lower airway colonization and inflammatory response in COPD: a focus on Haemophilus influenzae. Int J Chron Obstruct Pulmon Dis. 2014;9:1119–1132. PubMed PMID: 25342897.

[34] Sethi S, Evans N, Grant BJ, et al. New strains of bacteria and exacerbations of chronic obstructive pulmonary disease. N Engl J Med. 2002 Aug 15;347 (7):465–471. PubMed PMID: 12181400.

[35] Sethi S, Wrona C, Eschberger K, et al. Inflammatory profile of new bacterial strain exacerbations of chronic obstructive pulmonary disease. Am J Respir Crit Care Med. 2008 Mar 1;177(5):491–497. PubMed PMID: 18079493.

[36] Anzueto A. Impact of exacerbations on COPD. Eur Respir Rev. 2010 Jun;19(116):113–118. PubMed PMID: 20956179.

[37] Desai H, Eschberger K, Wrona C, et al. Bacterial colonization increases daily symptoms in patients with chronic obstructive pulmonary disease. Ann Am Thorac Soc. 2014 Mar;11(3):303–309. PubMed PMID: 24423399.

[38] Murphy TF, Brauer AL, Schiffmacher AT, et al. Persistent colonization by Haemophilus influenzae in chronic obstructive pulmonary disease. Am J Respir Crit Care Med. 2004 Aug 1;170(3):266–272. PubMed PMID: 15117742.

[39] Loeb MR. Ferrochelatase activity and protoporphyrin IX utilization in Haemophilus influenzae. J Bacteriol. 1995 Jun;177(12):3613–3615. PubMed PMID: 7768877.

[40] Schlor S, Herbert M, Rodenburg M, et al. Characterization of ferrochelatase (hemH) mutations in Haemophilus influenzae. Infect Immun. 2000 May;68(5):3007–3009. PubMed PMID: 10769004.

[41] Granick S, Gilder H. The porphyrin requirements of Haemophilus influenzae and some functions of the vinyl and propionic acid side chains of heme. J Gen Physiol. 1946 Sep;30:1–13. PubMed PMID: 20997746.

[42] Morton DJ, Smith A, Ren Z, et al. Identification of a haem-utilization protein (Hup) in Haemophilus influenzae. Microbiology. 2004 Dec;150(Pt 12):3923–3933. PubMed PMID: 15583146.

[43] LaCross NC, Marrs CF, Gilsdorf JR. Otitis media associated polymorphisms in the hemin receptor HemR of nontypeable Haemophilus influenzae. Infect Genet Evol. 2014 Aug;26:47–57. PubMed PMID: 24820341.

[44] Jin H, Ren Z, Pozsgay JM, et al. Cloning of a DNA fragment encoding a heme-repressible hemoglobin-binding outer membrane protein from *Haemophilus influenzae*. Infect Immun. 1996 Aug;64 (8):3134–3141. PubMed PMID: 8757844.

[45] Jin H, Ren Z, Whitby PW, et al. Characterization of *hgpA*, a gene encoding a haemoglobin/haemoglobin--haptoglobin-binding protein of *Haemophilus influenzae*. Microbiology. 1999 Apr;145(Pt 4):905–914. PubMed PMID: 10220170.

[46] Maciver I, Latimer JL, Liem HH, et al. Identification of an outer membrane protein involved in utilization of hemoglobin-haptoglobin complexes by nontypeable *Haemophilus influenzae*. Infect Immun. 1996 Sep;64 (9):3703–3712. PubMed PMID: 8751920.

[47] Morton DJ, Bakaletz LO, Jurcisek JA, et al. Reduced severity of middle ear infection caused by nontypeable *Haemophilus influenzae* lacking the hemoglobin/hemoglobin-haptoglobin binding proteins (Hgp) in a chinchilla model of otitis media. Microb Pathog. 2004 Jan;36(1):25–33. PubMed PMID: 14643637.

[48] Morton DJ, Whitby PW, Jin H, et al. Effect of multiple mutations in the hemoglobin- and hemoglobin-haptoglobin-binding proteins, HgpA, HgpB, and HgpC, of *Haemophilus influenzae* type b. Infect Immun. 1999 Jun;67(6):2729–2739. PubMed PMID: 10338475.

[49] Ren Z, Jin H, Morton DJ, et al. *hgpB*, a gene encoding a second *Haemophilus influenzae* hemoglobin- and hemoglobin-haptoglobin-binding protein. Infect Immun. 1998 Oct;66(10):4733–4741. PubMed PMID: 9746572.

[50] Seale TW, Morton DJ, Whitby PW, et al. Complex role of hemoglobin and hemoglobin-haptoglobin binding proteins in *Haemophilus influenzae* virulence in the infant rat model of invasive infection. Infect Immun. 2006 Nov;74(11):6213–6225. PubMed PMID: 16966415.

[51] Cope LD, Love RP, Guinn SE, et al. Involvement of HxuC outer membrane protein in utilization of hemoglobin by *Haemophilus influenzae*. Infect Immun. 2001 Apr;69(4):2353–2363. PubMed PMID: 11254593.

[52] Cope LD, Thomas SE, Hrkal Z, et al. Binding of heme-hemopexin complexes by soluble HxuA protein allows utilization of this complexed heme by *Haemophilus influenzae*. Infect Immun. 1998 Sep;66 (9):4511–4516. PubMed PMID: 9712810.

[53] Fournier C, Smith A, Delepelaire P. Haem release from haemopexin by HxuA allows *Haemophilus influenzae* to escape host nutritional immunity. Mol Microbiol. 2011 Apr;80(1):133–148. PubMed PMID: 21276097.

[54] Hanson MS, Pelzel SE, Latimer J, et al. Identification of a genetic locus of *Haemophilus influenzae* type b necessary for the binding and utilization of heme bound to human hemopexin. Proc Natl Acad Sci U S A. 1992 Mar 01;89(5):1973–1977. PubMed PMID: 1542695.

[55] Morton DJ, Seale TW, Madore LL, et al. The haem-haemopexin utilization gene cluster (*hxuCBA*) as a virulence factor of *Haemophilus influenzae*. Microbiology. 2007 Jan;153(Pt 1):215–224. PubMed PMID: 17185550.

[56] Wong JC, Patel R, Kendall D, et al. Affinity, conservation, and surface exposure of hemopexin-binding proteins in *Haemophilus influenzae*. Infect Immun. 1995 Jun;63(6):2327–2333. PubMed PMID: 7768617.

[57] Hanson MS, Slaughter C, Hansen EJ. The *hbpA* gene of *Haemophilus influenzae* type b encodes a heme-binding lipoprotein conserved among heme-dependent *Haemophilus* species. Infect Immun. 1992 Jun;60(6):2257–2266. PubMed PMID: 1339409.

[58] Mason KM, Raffel FK, Ray WC, et al. Heme utilization by nontypeable *Haemophilus influenzae* is essential and dependent on Sap transporter function. J Bacteriol. 2011 May;193(10):2527–2535. PubMed PMID: 21441512.

[59] Morton DJ, Madore LL, Smith A, et al. The heme-binding lipoprotein (HbpA) of *Haemophilus influenzae*: role in heme utilization. FEMS Microbiol Lett. 2005 Dec 15;253(2):193–199. PubMed PMID: 16289530.

[60] Morton DJ, Seale TW, Bakaletz LO, et al. The heme-binding protein (HbpA) of *Haemophilus influenzae* as a virulence determinant. Int J Med Microbiol. 2009 Nov;299(7):479–488. PubMed PMID: 19451029.

[61] Morton DJ, Seale TW, Vanwagoner TM, et al. The *dppBCDF* gene cluster of *Haemophilus influenzae*: role in heme utilization. BMC Res Notes. 2009 Aug 24;2:166. PubMed PMID: 19703293.

[62] Vergauwen B, Elegheert J, Dansercoer A, et al. Glutathione import in *Haemophilus influenzae* Rd is primed by the periplasmic heme-binding protein HbpA. Proc Natl Acad Sci U S A. 2010 Jul 27;107 (30):13270–13275. PubMed PMID: 20628015.

[63] Al Jubair T, Singh B, Fleury C, et al. *Haemophilus influenzae* stores and distributes hemin by using protein E. Int J Med Microbiol. 2014 Jul;304(5–6):662–668. PubMed PMID: 24863527.

[64] Szelestey BR, Heimlich DR, Raffel FK, et al. *Haemophilus* responses to nutritional immunity: epigenetic and morphological contribution to biofilm architecture, invasion, persistence and disease severity. PLoS Pathog. 2013;9(10):e1003709. PubMed PMID: 24130500.

[65] van Zundert GCP, Rodrigues J, Trellet M, et al. The HADDOCK2.2 web server: user-friendly integrative modeling of biomolecular complexes. J Mol Biol. 2016 Feb 22;428(4):720–725. PubMed PMID: 26410586.

[66] Wassenaar TA, Van Dijk M, Loureiro-Ferreira N, et al. WeNMR: Structural biology on the grid. J Grid Comput. 2012;10(4):743–767.

[67] Roy A, Kucukural A, Zhang Y. I-TASSER: a unified platform for automated protein structure and function prediction. Nat Protoc. 2010 Apr;5(4):725–738. PubMed PMID: 20360767.

[68] Zhang Y. I-TASSER server for protein 3D structure prediction. BMC Bioinformatics. 2008 Jan 23;9:40. PubMed PMID: 18215316.

[69] Yang J, Roy A, Zhang Y. Protein-ligand binding site recognition using complementary binding-specific

substructure comparison and sequence profile alignment. Bioinformatics. 2013 Oct 15;29 (20):2588–2595. PubMed PMID: 23975762.

[70] Yang J, Roy A, Zhang Y. BioLiP: a semi-manually curated database for biologically relevant ligand-protein interactions. Nucleic Acids Res. 2013 Jan;41(Database issue):D1096–103. PubMed PMID: 23087378.

[71] Laskowski RA, Swindells MB. LigPlot+: multiple ligand-protein interaction diagrams for drug discovery. J Chem Inf Model. 2011 Oct 24;51 (10):2778–2786. PubMed PMID: 21919503.

[72] Herriott RM, Meyer EY, Vogt M, et al. Defined medium for growth of *Haemophilus influenzae*. J Bacteriol. 1970 Feb;101(2):513–516. PubMed PMID: 5308770.

[73] Vergauwen B, Pauwels F, Vaneechoutte M, et al. Exogenous glutathione completes the defense against oxidative stress in *Haemophilus influenzae*. J Bacteriol. 2003 Mar;185(5):1572–1581. PubMed PMID: 12591874.

[74] Allen S, Zaleski A, Johnston JW, et al. Novel sialic acid transporter of *Haemophilus influenzae*. Infect Immun. 2005 Sep;73(9):5291–5300. PubMed PMID: 16113244.

[75] Tracy E, Ye F, Baker BD, et al. Construction of non-polar mutants in *Haemophilus influenzae* using FLP recombinase technology. BMC Mol Biol.2008 Nov 11;9:101. PubMed PMID: 19014437.

[76] Sinha S, Mell JC, Redfield RJ. Seventeen Sxy-dependent cyclic AMP receptor protein site-regulated genes are needed for natural transformation in *Haemophilus influenzae*. J Bacteriol. 2012 Oct;194(19):5245–5254. PubMed PMID: 22821979.

[77] Herriott RM, Meyer EM, Vogt M. Defined nongrowth media for stage II development of competence in *Haemophilus influenzae*. J Bacteriol. 1970 Feb;101 (2):517–524. PubMed PMID: 5308771.

[78] Clinical & Laboratory Standards Institute. CSLI Guidelines. Performance Standards for Antimicrobial Susceptibility Testing: 27th Edition. CLSI M100-S27. 2017.

[79] Euba B, Lopez-Lopez N, Rodriguez-Arce I, et al. Resveratrol therapeutics combines both antimicrobial and immunomodulatory properties against respiratory infection by nontypeable *Haemophilus influenzae*. Sci Rep. 2017 Oct 16;7(1):12860. PubMed PMID: 29038519. DOI:10.1038/s41598-017-13034-7.

[80] Euba B, Moleres J, Segura V, et al. Genome expression profiling-based identification and administration efficacy of host-directed antimicrobial drugs against respiratory infection by nontypeable *Haemophilus influenzae*. Antimicrob Agents Chemother. 2015 Dec;59(12):7581–7592. PubMed PMID: 26416856.

[81] Euba B, Moleres J, Viadas C, et al. Relationship between azithromycin susceptibility and administration efficacy for nontypeable *Haemophilus influenzae* respiratory infection. Antimicrob Agents Chemother. 2015 May;59(5):2700–2712. PubMed PMID: 25712355.

[82] Euba B, Moleres J, Viadas C, et al. Relative contribution of P5 and Hap surface proteins to nontypeable *Haemophilus influenzae* interplay with the host upper

and lower airways. PLoS One. 2015;10(4):e0123154. PubMed PMID: 25894755.

[83] Lopez-Gomez A, Cano V, Moranta D, et al. Host cell kinases, α5 and β1 integrins, and Rac1 signalling on the microtubule cytoskeleton are important for non-typeable *Haemophilus influenzae* invasion of respiratory epithelial cells. Microbiology. 2012 Sep;158(Pt 9):2384–2398. PubMed PMID: 22723286.

[84] Morey P, Cano V, Marti-Lliteras P, et al. Evidence for a non-replicative intracellular stage of nontypeable *Haemophilus influenzae* in epithelial cells. Microbiology. 2011 Jan;157(Pt 1):234–250. PubMed PMID: 20929955.

[85] Morey P, Viadas C, Euba B, et al. Relative contributions of lipooligosaccharide inner and outer core modifications to nontypeable *Haemophilus influenzae* pathogenesis. Infect Immun. 2013 Nov;81 (11):4100–4111. PubMed PMID: 23980106.

[86] Rodriguez-Arce I, Marti S, Euba B, et al. Inactivation of the thymidylate synthase *thyA* in non-typeable *Haemophilus influenzae* modulates antibiotic resistance and has a strong impact on its interplay with the host airways. Front Cell Infect Microbiol. 2017;7:266. PubMed PMID: 28676846.

[87] Grillo MJ, Blasco JM, Gorvel JP, et al. What have we learned from brucellosis in the mouse model? Vet Res.2012 Apr 13;43:29. PubMed PMID: 22500859; PubMed Central PMCID: PMCPMC3410789.

[88] Dunten P, Mowbray SL. Crystal structure of the dipeptide binding protein from *Escherichia coli* involved in active transport and chemotaxis. Protein Sci. 1995 Nov;4(11):2327–2334. PubMed PMID: 8563629.

[89] Dunten P, Mowbray SL. Modeling of the structure of the *Haemophilus influenzae* heme-binding protein suggests a mode of heme interaction. Protein Sci. 1995 Nov;4(11):2335–2340. PubMed PMID: 8563630.

[90] Tanaka KJ, Pinkett HW. Oligopeptide-binding protein from nontypeable *Haemophilus influenzae* has ligand-specific sites to accommodate peptides and heme in the binding pocket. J Biol Chem.2019 Jan 18;294(3):1070–1082. PubMed PMID: 30455346.

[91] Singh B, Al-Jubair T, Morgelin M, et al. The unique structure of *Haemophilus influenzae* protein E reveals multiple binding sites for host factors. Infect Immun. 2013 Mar;81(3):801–814. PubMed PMID: 23275089.

[92] Zambolin S, Clantin B, Chami M, et al. Structural basis for haem piracy from host haemopexin by *Haemophilus influenzae*. Nat Commun.2016 May 18;7:11590. PubMed PMID: 27188378.

[93] Whitby PW, Sim KE, Morton DJ, et al. Transcription of genes encoding iron and heme acquisition proteins of *Haemophilus influenzae* during acute otitis media. Infect Immun. 1997 Nov;65(11):4696–4700. PubMed PMID: 9353052.

[94] Stauff DL, Skaar EP. The heme sensor system of *Staphylococcus aureus*. Contrib Microbiol. 2009;16:120–135. PubMed PMID: 19494582.

[95] Whitby PW, Seale TW, VanWagoner TM, et al. The iron/heme regulated genes of *Haemophilus influenzae*: comparative transcriptional profiling as a tool to define the species core modulon. BMC Genomics.2009 Jan 07;10:6. PubMed PMID: 19128474.

[96] Whitby PW, Vanwagoner TM, Seale TW, et al. Transcriptional profile of *Haemophilus influenzae*: effects of iron and heme. J Bacteriol. 2006 Aug;188 (15):5640–5645. PubMed PMID: 16855256.

[97] Fleischmann RD, Adams MD, White O, et al. Whole-genome random sequencing and assembly of *Haemophilus influenzae* Rd. Science.1995 Jul 28;269 (5223):496–512. PubMed PMID: 7542800.

[98] Adhikari P, Kirby SD, Nowalk AJ, et al. Biochemical characterization of a *Haemophilus influenzae* periplasmic iron transport operon. J Biol Chem.1995 Oct 20;270(42):25142–25149. PubMed PMID: 7559648.

[99] Anderson DS, Adhikari P, Nowalk AJ, et al. The hFbpABC transporter from *Haemophilus influenzae* functions as a binding-protein-dependent ABC transporter with high specificity and affinity for ferric iron. J Bacteriol. 2004 Sep;186(18):6220–6229. PubMed PMID: 15342592.

[100] Anderson DS, Adhikari P, Weaver KD, et al. The *Haemophilus influenzae* hFbpABC Fe3+ transporter: analysis of the membrane permease and development of a gallium-based screen for mutants. J Bacteriol. 2007 Jul;189(14):5130–5141. PubMed PMID: 17496104.

[101] Sanders JD, Cope LD, Hansen EJ. Identification of a locus involved in the utilization of iron by *Haemophilus influenzae*. Infect Immun. 1994 Oct;62 (10):4515–4525. PubMed PMID: 7927717.

[102] Mason KM, Bruggeman ME, Munson RS, et al. The non-typeable *Haemophilus influenzae* Sap transporter provides a mechanism of antimicrobial peptide resistance and SapD-dependent potassium acquisition. Mol Microbiol. 2006 Dec;62(5):1357–1372. PubMed PMID: 17064364.

[103] Mason KM, Munson RS Jr., Bakaletz LO. A mutation in the *sap* operon attenuates survival of nontypeable *Haemophilus influenzae* in a chinchilla model of otitis media. Infect Immun. 2005 Jan;73(1):599–608. PubMed PMID: 15618200.

[104] Raffel FK, Szelestey BR, Beatty WL, et al. The *Haemophilus influenzae* Sap transporter mediates bacterium-epithelial cell homeostasis. Infect Immun. 2013 Jan;81(1):43–54. PubMed PMID: 23071138.

[105] Ronander E, Brant M, Eriksson E, et al. Nontypeable *Haemophilus influenzae* adhesin protein E: characterization and biological activity. J Infect Dis.2009 Feb 15;199(4):522–531. PubMed PMID: 19125675.

[106] Ronander E, Brant M, Janson H, et al. Identification of a novel *Haemophilus influenzae* protein important for adhesion to epithelial cells. Microbes Infect. 2008 Jan;10(1):87–96. PubMed PMID: 18069033.

[107] Morris D, Khurasany M, Nguyen T, et al. Glutathione and infection. Biochim Biophys Acta. 2013 May;1830 (5):3329–3349. PubMed PMID: 23089304.

[108] Sporer AJ, Kahl LJ, Price-Whelan A, et al. Redox-based regulation of bacterial development and behavior. Annu Rev Biochem.2017 Jun 20;86:777–797. PubMed PMID: 28654321.

[109] Huang W, Wilks A. Extracellular heme uptake and the challenge of bacterial cell membranes. Annu Rev Biochem.2017 Jun 20;86:799–823. PubMed PMID: 28426241.

[110] Carver PL. The battle for iron between humans and microbes. PubMed PMID: 28730969 Curr Med Chem. 2018;25(1):85–96.

[111] Shepherd M, Heath MD, Poole RK. NikA binds heme: a new role for an *Escherichia coli* periplasmic nickel-binding protein. Biochemistry.2007 May 1;46 (17):5030–5037. PubMed PMID: 17411076.

[112] Shelton CL, Raffel FK, Beatty WL, et al. Sap transporter mediated import and subsequent degradation of antimicrobial peptides in *Haemophilus*. PLoS Pathog. 2011 Nov;7(11):e1002360. PubMed PMID: 22072973.

[113] Garmendia J, Viadas C, Calatayud L, et al. Characterization of nontypeable *Haemophilus influenzae* isolates recovered from adult patients with underlying chronic lung disease reveals genotypic and phenotypic traits associated with persistent infection. PLoS One. 2014;9(5):e97020. PubMed PMID: 24824990.

[114] Hardison RLHD, Harrison A, Beatty WL, et al. Transient nutrient deprivation promotes macropinocytosis-dependent intracellular bacterial community development. mSphere. 2018;3(5):e00286–18.

[115] Vogel AR, Szelestey BR, Raffel FK, et al. SapF-mediated heme-iron utilization enhances persistence and coordinates biofilm architecture of *Haemophilus*. Front Cell Infect Microbiol. 2012;2:42. PubMed PMID: 22919633.

[116] Gawronski JD, Wong SM, Giannoukos G, et al. Tracking insertion mutants within libraries by deep sequencing and a genome-wide screen for *Haemophilus* genes required in the lung. Proc Natl Acad Sci U S A.2009 Sep 22;106(38):16422–16427. PubMed PMID: 19805314.

[117] Hood DW, Makepeace K, Deadman ME, et al. Sialic acid in the lipopolysaccharide of *Haemophilus influenzae*: strain distribution, influence on serum resistance and structural characterization. Mol Microbiol. 1999 Aug;33(4):679–692. PubMed PMID: 10447878.